NWL Report No. 1786
NAVWEPS Report No. 7669

EXPLOSIVE-INDUCED PRESSURES IN IRON

by

William G. Soper
and
Lester A. Potteiger
Warhead and Terminal Ballistics Laboratory

U. S. NAVAL WEAPONS LABORATORY
DAHLGREN, VIRGINIA

Date: 22 November 1961

U. S. Naval Weapons Laboratory
Dahlgren, Virginia

Explosive-Induced Pressures in Iron

by

William G. Soper
and
Lester A. Potteiger
Warhead and Terminal Ballistics Laboratory

NWL Report No. 1786
NAVWEPS Report No. 7669

BUWEPS Task Assignment No.
R01101001

22 November 1961

CONTENTS

ABSTRACT

A metallographic technique is discussed for determining the level of pressure to which iron plates have been subjected by explosive loading. The interaction of the shock and rarefaction waves within the plate is analyzed to arrive at formulas from which the intensity of pressure can be determined when the velocity of the detonation front is known. This technique is employed to determine the pressure induced in iron by oblique detonation of four common explosives, Compositions B, C-3, C-4, and H-6.

FOREWORD

This report was prepared under the BUWEPS Foundational Research Task No. R01101001. The experimental data were obtained from studies conducted under the NWL Foundational Research Task No. 12014. The subject matter concerns the interaction between a detonating high explosive and a confining medium. The contents of the report are pertinent to the fields of explosives research, high-pressure physics, and ordnance design.

This report was reviewed by:

J. C. TALLEY, Head, Research Division
Warhead and Terminal Ballistics Laboratory
C. B. GREEN, Director
Warhead and Terminal Ballistics Laboratory
R. H. LYDDANE, Technical Director
U. S. Naval Weapons Laboratory

APPROVED FOR RELEASE:

/s/ R. H. LYDDANE
Technical Director

I. INTRODUCTION

It is by now well established that two distinct shock waves are produced in an iron specimen subjected to explosive loading in the range of 131 to 340 kilobars [1, 2]*. It is also well known that this shock system changes the hardness of the specimen. By examination of the sectioned specimen after test, it is possible to determine the meeting point of the slower, high-pressure shock and the reflection of the faster shock from the free surface. This interaction zone appears as a near discontinuity in the hardness across the thickness of the specimen. The zone can be detected by a hardness traverse or by etching and visual examination.

Smith [2, 3] has shown that the location of the interaction zone can be used to compute the magnitude of the pressure applied to iron specimens by explosives. Smith's work, however, is restricted to the case of normal incidence of the detonation wave. This report extends these concepts to the case of oblique loading, in which the detonation front sweeps along one face of an iron plate at constant velocity. Equations are derived relating the induced pressure to the disturbance velocity and the location of the interaction zone. Also, the results of a series of oblique-wave experiments are analyzed by this method to yield values of induced pressure for several common explosives.

II. INTERACTION ZONE FORMATION BY OBLIQUE LOADING

This section will develop the theory of interaction zone formation for a pressure wave of constant magnitude. The following section will relate these results to loading by detonation waves. The problem is illustrated in Figure 1. A disturbance sweeps along the plate, generating in the plate two shock waves which travel with different velocities. The first shock wave reflects at the free surface as a rarefaction wave. This rarefaction returns to intersect the oncoming second shock wave and form the interaction zone. The analysis will employ a coordinate system in which the disturbance front is stationary. The symbols to be used are defined below.

x = coordinate parallel to undisturbed interface

y = coordinate perpendicular to undisturbed interface

V = velocity of disturbance along x-axis

θ_1, θ_2 = angles of first and second shock waves relative to x-axis

*Numbers in brackets refer to References.

θ_3 = angle of interface relative to x-axis

θ_4 = angle of rarefaction wave relative to undisturbed free surface

u_1 = particle velocity change produced by first shock wave

u_2 = particle velocity change produced by second shock wave

U_1 = velocity of first shock wave relative to undisturbed material

U_2 = velocity of second shock wave relative to material ahead of the wave

R = average rarefaction velocity relative to material ahead of rarefaction wave

V_1 = velocity of flow between shock waves

ϕ = angle of flow between shock waves, relative to x-axis

P_1 = pressure behind first shock wave

P_2 = pressure behind second shock wave

v_o = initial specific volume of metal

v_1 = specific volume behind first shock wave

v_2 = specific volume behind second shock wave

The objective of the analysis is to express the pressure applied to the metal, P_2, in terms of the interaction zone location. In distinction to the case of normal loading, the disturbance velocity, V, also appears in the relationship. It is most convenient to compute and tabulate this relationship by first assuming values for P_2 and V and then calculating the zone location.

The velocities U_1 and u_1 are given by reference 1 as 5.05 $\frac{mm}{\mu sec}$ and .32 $\frac{mm}{\mu sec}$, respectively.

The velocities U_2 and u_2 are expressible as follows [2]:

$$U_2 = v_1\sqrt{\frac{P_2 - P_1}{v_1 - v_2}} \qquad u_2 = \sqrt{(P_2 - P_1)(v_1 - v_2)}$$

The specific volumes v_1 and v_2, corresponding to pressures P_1 and P_2, are defined by the Hugoniot function, Fig. 2. In this paper, values of 131 kb and .936 are used for P_1 and v_1/v_o, respectively. From Fig. 2 and the foregoing equations, the quantities U_2 and u_2 can be computed for any specific P_2.

The angle θ_1 is determined by the condition that the component of V normal to the shock wave must equal the shock velocity:

$$V \sin \theta_1 = U_1 \qquad \theta_1 = \sin^{-1} U_1/V$$

Upon crossing the first shock, the velocity component normal to the front is reduced by the amount u_1. The tangential component is unaffected by the shock. The quantities ϕ and V_1 are therefore given by

$$\phi = \theta_1 - \tan^{-1}\left(\frac{U_1 - u_1}{V \cos \theta_1}\right)$$

$$V_1^2 = (V \cos \theta_1)^2 + (U_1 - u_1)^2$$

The angles θ_2 and θ_4 are determined by the condition that the flow velocity normal to the respective wave fronts must be equal to the wave velocities:

$$V_1 \sin (\theta_2 - \phi) = U_2 \qquad \theta_2 = \sin^{-1}\left(\frac{U_2}{V_1}\right) + \phi$$

and

$$V_1 \sin (\theta_4 + \phi) = R \qquad \theta_4 = \sin^{-1}\left(\frac{R}{V_1}\right) - \phi$$

A value of 4.95 $\frac{mm}{\mu sec}$ is used for R in this paper. This is the average of velocities of the head and tail of the rarefaction wave as given in reference 3 when adjustments are made for the difference in coordinates. The average rarefaction velocity is used here because it is expected that this procedure will produce the best estimate of the location of the center of the interaction zone. It is realized that the wave pattern during interaction is complex and, in particular, that the velocity of the shock wave does not remain constant after interaction begins. The use of a constant shock velocity within the region covered by the rarefaction wave in Fig. 1 is therefore an approximation.

The location of the interaction zone can be determined for specific P_2 and V from calculated values of θ_1, θ_2, θ_4, and ϕ. The configuration is shown in Fig. 3, where the location of the interaction zone relative to the surface of the plate adjacent to the explosive is defined by the length a. The line of metal particles which forms the center of the interaction zone crosses the first shock and moves at an angle ϕ toward the intersection of the rarefaction and the second shock. Defining an auxiliary set of lengths c, d, and e, the geometry of Fig. 3 yields the following equations:

$$d \cos \theta_2 = c \cos \theta_1 + e \cos \theta_4$$

$$h = c \sin \theta_1 \qquad h = e \sin \theta_4 + d \sin \theta_2$$

$$\tan \phi = \frac{(h-a) - e \sin \theta_4}{c \cos \theta_1 + e \cos \theta_4 - \frac{a}{\tan \theta_1}}$$

The above equations may be solved for h/a in terms of the known angles:

$$\frac{h}{a} = \frac{\sin \theta_1 \cos \theta_2 - \sin \theta_2 \cos \theta_1}{\sin \theta_1 \cos \theta_4 + \sin \theta_4 \cos \theta_1} \qquad \frac{\tan \phi \cos \theta_4 + \sin \theta_4}{\sin \theta_2 - \tan \phi \cos \theta_2} + 1$$

The above equation was used to plot P_2 as a function of a/h and V in Fig. 4. It is worthwhile to note that the curve for normal incidence, calculated from reference 3, must be the limiting curve for oblique incidence as the velocity V approaches infinity. Fig. 4 shows that a velocity of 15 $\frac{mm}{\mu sec}$ is essentially "infinite" as far as the value of a/h is concerned. The velocity of 5.44 $\frac{mm}{\mu sec}$ is the minimum velocity for which the analysis presented in this report is valid. At this value of V, the flow behind the first shock wave becomes sonic; i.e., the magnitude of the flow velocity, V_1, becomes equal to the local sound speed, 5.15 $\frac{mm}{\mu sec}$. For velocities below 5.44 $\frac{mm}{\mu sec}$, the diagram in Fig. 1 will no longer describe the wave pattern in the plate, since the influence of the free surface will no longer be confined to a region downstream of the first shock wave.

It is also possible to derive the angle of interface deflection θ_3, in terms of a/h and V. Upon crossing the second shock, the normal component of velocity is reduced by the particle velocity, u_2, appropriate to that shock. The resulting flow must be parallel to the interface, and the angle of the flow relative to x is therefore θ_3. The appropriate equation is as follows:

$$\theta_3 = \theta_2 - \tan^{-1}\left[\frac{U_2 - u_2}{V_1 \cos(\theta_2 - \phi)}\right]$$

Fig. 5 presents the relationship between θ_3, a/h, and V. Normal incidence produces no interface rotation, and θ_3 is zero when $V = \infty$. For this case, the minimum value of a/h is .537, corresponding to an applied pressure of 131 kb. Thus, the limit curve for $V = \infty$ is the portion of the horizontal axis between a/h = .537 and a/h = 1.

III. OBLIQUE DETONATION WAVES

Before the theory of the previous section can be applied to loading by explosives, it is necessary to examine the nature of oblique detonation waves in some detail. For this purpose, we will employ the familiar detonation wave model consisting of a surface upon which all variables have Chapman-Jouguet values, followed by a region in which pressure monotonically decreases toward zero. Such a model ignores the finite reaction zone which must precede the Chapman-Jouguet surface. A portion of the wave pattern induced in an iron plate by this detonation wave is shown in Fig. 6 for two distinctly different cases.

Case 1 in Fig. 6 is very similar to the situation discussed in Section II. The only difference arises from the fact that the pressure behind the detonation front is not constant, but is diminishing with distance along the interface. The decreasing pressure produces a rarefaction wave which interacts with the second shock wave in the iron, lowering the peak pressure, and therefore the velocity, of the shock. The second shock front is consequently not straight, and the location of the interaction zone is not simply related to the induced pressure.

In Case 2, a fundamentally different phenomenon occurs. Here the induced pressure along the interface is assumed to vary in the same manner as in Case 1, but the plate is thicker. When the pressure at the interface decays to 131 kb, a rarefaction shock [5] is produced. This shock is formed because rarefaction velocities for pressures below 131 kb exceed those for pressures immediately above 131 kb. The lower-pressure rarefaction wavelets move into the metal

and overtake wavelets associated with the higher pressures, creating a discontinuity in the flow variables. This rarefaction shock eventually overtakes the second shock wave and annihilates it. The streamline upon which this interaction occurs separates the plate into two regions, one having experienced higher pressures than the other. It would thus be expected that a discontinuity in hardness similar to that observed in Case 1 will occur here also.

From the foregoing discussion, the hardened zone thickness, a, is expected to vary with plate thickness, h, in the following manner, the explosive thickness being constant: For very thick plates, a is independent of h. As h is reduced, however, a point is reached at which a abruptly begins to diminish. Because of the curvature of the second shock in Fig. 6, the rate of decrease of a increases as h becomes smaller. As h approaches zero, the interaction of the second shock and the reflected rarefaction occurs under conditions which approach those assumed in Section II; i.e., constant pressure behind the second shock and a straight second shock front. It follows that the peak pressure induced in the metal, which is the pressure associated with the front of the detonation wave, can be found by determining the limiting value of a/h as h tends to zero and employing this quantity in the analysis of Section II.

As a final point of interest, it is worthwhile to consider the influence of explosive thickness upon the a(h) relation discussed in the preceding paragraph. The necessary relations can be conveniently found from dimensional analysis. For Case 1 of Fig. 6, the quantity a depends upon the following variables:

P_{cj} = Chapman-Jouguet pressure of explosive

ρ = density of explosive

D = detonation velocity of explosive

S = any coefficient in the function $P(v/v_o)$ representing Hugoniot curve for iron

ℓ = explosive thickness

h = plate thickness

The first 3 variables completely characterize the explosive. Definitions of other explosive parameters in terms of these quantities are given in reference 6. The quantity S requires brief explanation: Consider the Hugoniot curve for iron expressed exactly as a function of v/v_o. This is always possible conceptually, although in practice the function may be very complex. Since the function contains only the variables P and v/v_o, and since v/v_o is dimensionless while P has dimensions of pressure, it follows that all coefficients occurring in the function must have dimensions of pressure or be dimensionless. The set of these coefficients then characterizes the material, and a typical coefficient is represented by S.

Proceeding with the formation of dimensionless variables, the following results:

$$\frac{a}{\ell} = f\left(\frac{h}{\ell}, \frac{S}{P_{cj}}, \rho\frac{D^2}{P_{cj}}\right)$$

where f denotes "a function of". Since we are considering only one metal and one explosive, $\frac{S}{P_{cj}}$ and $\rho\frac{D^2}{P_{cj}}$ are constants. Under these conditions, then, $\frac{a}{\ell}$ is a function of $\frac{h}{\ell}$. This is the desired result; the a(h) relation for an explosive thickness of ℓ_2 can be found from that for a thickness of ℓ_1 by multiplying both ordinate and abscissa by the factor ℓ_2/ℓ_1. In the common terminology, the solution is said to "scale".

In Case 2 of Fig. 6, a does not depend upon h. The appropriate relationship therefore is

$$\frac{a}{\ell} = f\left(\frac{S}{P_{cj}}, \rho\frac{D^2}{P_{cj}}\right)$$

For a specific metal-explosive combination, the function on the right is constant, and a is given by

$$a = \text{constant} \times \ell$$

This shows that the maximum hardened zone thickness is directly proportional to explosive thickness.

A later section of this report will present experimental data on hardened zones for various explosives and plate thicknesses. These data will be plotted on $a/\ell - h/\ell$ coordinates for comparison with the theory developed here.

IV. EXPERIMENTS

A number of experiments were performed in which iron and steel plates were subjected to oblique loading by four different explosives. The explosives employed in the experiments are listed in Table I. Included are the compositions, measured densities, and estimated detonation velocities. The references from which the detonation velocities were determined are given in parentheses:

TABLE I CHARACTERISTICS OF EXPLOSIVES

Explosive	Composition	Density [gm/cc]	Detonation Velocity [mm/μsec]
Comp B	60/40, RDX/TNT	1.71	7.9 (7)
C-3	77/10/5/4/3/1 RDX/DNT/MNT/TNT/ Tetryl/Nitrocellulose	1.57	7.6 (8)
C-4	91/9, RDX/Plasticizer	1.40	7.3 (8)
H-6	45/30/20/5, RDX/TNT/ Aluminum/Wax	1.78	7.2 (9)

Fig. 7 shows the experimental arrangement. Initiation of the plastic explosives was provided by a series of detonators located along one edge of the slab. For the cast explosives, the detonators were placed in an auxiliary slab of plastic explosive (Composition C-3) which abutted the main slab. In all cases, the maximum spacing of the detonators was 1.5". In the experiments, the metal thickness was varied from .2" to 1". The explosive thickness was set at 1" for all explosives except Composition C-3. For C-3, the explosive thickness was varied from .25" to 2".

After test, the plates were sectioned longitudinally along the center line and etched to render the interaction zone visible. It was observed that the hardened region varied in thickness for the first 2" of detonation wave travel but then attained a constant value. Certain plates were sectioned laterally as well as longitudinally. It was found that the uniform hardened region extended to within 1-1/2 plate thicknesses of the lateral edges. From these results it was concluded that the central portions of the plates experienced steady detonation conditions and were free from lateral expansion effects during the formation of the interaction zone. There was, however, in many plates a reduction in thickness as a result of lateral expansion occurring at later times. This reduction was generally less than 5% for explosive thicknesses of 1" or less but attained values of approximately 10% for some of the thicker C-3 tests. It was also observed that some plates contained internal cracks and spalls which produced a final thickness greater than the original. The deformation of the plates necessitated a correction of the measured hardened zone thicknesses; the measured thicknesses were multiplied by the ratio of original plate thickness to final plate thickness. These corrected data are presented in Figures 8 and 9. All of the data from the tests are tabulated in Appendix A.

The iron plates used in these experiments were of Armco iron. The steel plates varied from type 1018 to type 1025, with carbon content ranging from .15% to .28%. There was no significant difference in the data from the iron and steel plates. For this reason the plate materials are not distinguished in Figures 8 and 9.

V. DISCUSSION

Figure 8 displays the data for Composition C-3 on a/ℓ - h/ℓ coordinates. The data are rather scattered, particularly for the smaller explosive thicknesses. To within the accuracy of the data, however, the results are completely consistent with the theory presented in Section III. The salient features are enumerated below:

1. The hardened zone thickness, a, "scales" with respect to explosive thickness, ℓ, and plate thickness, h; i.e., the ratio a/ℓ is a function only of the ratio h/ℓ.
2. a/ℓ is constant for large h/ℓ.
3. a/ℓ becomes dependent upon h/ℓ as h/ℓ is reduced, and the rate of decrease increases with decreasing h/ℓ.
4. The ratio a/h approaches a finite limit as h/ℓ tends to zero.

Figure 9 presents the data for the other explosives tested. The value of ℓ is 1 in. in all cases except those taken from reference 10. Again, the results are consistent with the theory of Section III. The only serious deviations appear in two points on the curves for C-4 and H-6, where the value of a/ℓ seems low. In view of the scatter shown by the more numerous data for C-3, however, it is felt that these discrepancies are attributable to experimental error and are not significant.

The data for Composition B from the experiments described in Section IV were not sufficient to define the plateau portion of the $a/\ell(h/\ell)$ relation. Fortunately, additional data were available from reference 10 for explosive thicknesses of .500, .504, .948, and 1.000 in. and plate thicknesses of approximately 2 in. Two of these data are shown in Figure 9. The other two lie near $h/\ell = 4$ and provide a/ℓ values of approximately .55. Thus, this independently obtained information supplements the results of these experiments and establishes that the variation of hard zone with plate thickness for Composition B is consistent with the theory of Section III.

The asymptotic values of a/h for small h/ℓ may be used with the analysis of Section II to obtain peak pressures induced in iron by oblique detonation waves in the various explosives. The estimated asymptotic slopes are indicated in Figures 8 and 9. Using the detonation velocities of Table 1 for the quantity V of Figure 4, the following table is obtained:

TABLE 2 PEAK INDUCED PRESSURES

Explosive	Asymptotic a/h	Pressure [kb]
Composition B	.725	180
C-3	.675	168
C-4	.720	185
H-6	.680	175

The accuracy of the calculated pressures is governed by the accuracies of the asymptotic slopes, a/h, and the detonation velocities, V. The possible error in the slopes is estimated from the scatter in the data of Figures 8 and 9 as ±5%. Reference to Fig. 4 shows that the resulting error in pressure is 8.5% at the point V = 8.00, P = 200.

Error in detonation velocity arises from the fact that V was not measured in the tests but was estimated from available detonation velocity data. These data relate to cylinders of explosive and not slabs of the sort employed in the experiments. It can be shown, however, that the error in V has only a small effect upon accuracy of the pressure. To obtain an order-of-magnitude estimate of the possible error in V, an equation relating detonation velocity in Composition B to charge diameter will be used [7]:

$$\text{detonation velocity}\left[\frac{\text{mm}}{\mu\text{sec}}\right] = 2.652 + 3.127 \times \text{density}\left[\frac{\text{gm}}{\text{cc}}\right] + .0134(\%\text{RDX}-65) - .151/\text{diameter [cm]}$$

The variation in velocity between a charge of 1 cm diameter and one of infinite diameter is .15 $\frac{\text{mm}}{\mu\text{sec}}$. Taking this as an estimate of the possible error in V for our problem, Fig. 4 yields an error in pressure of 1.5% at the point V = 8.00, P = 200. Combining the effects of errors in a/h and V, the maximum error of the pressures in Table 2 is estimated to be ±10%.

It is worthwhile to examine the plausibility of the computed peak pressures in the light of other data from the literature. Unfortunately, data for oblique loading are not too numerous. The following table lists information from several references:

TABLE 3 PEAK INDUCED PRESSURES FROM OTHER SOURCES

Reference	System	Explosive Density [gm/cc]	Detonation Velocity [mm/μsec]	Peak Pressure [kb]
11	63/37 Comp B Aluminum	1.67	7.868	168
11	63/37 Comp B Copper	1.67	7.868	188
12	60/40 Comp B Aluminum	1.73	8.0	178

TABLE 3 (Continued)

Reference	System	Explosive Density [gm/cc]	Detonation Velocity [mm/μsec]	Peak Pressure [kb]
13	Comp B - Aluminum	-	-	189
13	Comp B - Copper	-	-	205
13	Comp B - Iron	-	-	196
10	Comp B - Aluminum	-	7.62 - 7.95	195

In this table, all pressure values except the last were given by theoretical solutions of the problem of oblique loading. The last entry is based upon experimental data contained in reference 10. It was obtained by extrapolating to zero the data for peak pressure versus depth in plate. From these results, it appears that the pressures determined in this report by the interaction zone method are reasonable. The difference between the Comp B - Iron pressure from reference 13 and that presented in Table 2 is within experimental error.

VI. SUMMARY

Smith's method for determining explosive-induced pressures in iron by metallographic techniques is extended to include oblique loading. The peak pressure and the interface deflection angle are presented as functions of the detonation velocity and the location of the interaction zone. A series of experiments with four common explosives are described, and the peak pressures computed by this method compare satisfactorily with information from other sources.

For all systems investigated, the interaction zone location is found to scale with respect to the metal and explosive thicknesses. It is observed, under certain circumstances, that the interaction zone is formed by a rarefaction wave from the explosive-metal interface rather than by a rarefaction originating at the free surface of the metal.

VII. ACKNOWLEDGMENTS

The contributions of Messrs. J. W. Hagemeyer and W. Sturges, who planned many of the experiments, and Mr. F. D. Altman, who was responsible for the preparation of explosive charges, are gratefully acknowledged.

VIII. REFERENCES

1. D. Bancroft, E. L. Peterson, and S. Minshall, "Polymorphism of Iron at High Pressure," Journal of Applied Physics, 1956, vol. 27, pp. 291-298
2. C. S. Smith, "Metallographic Studies of Metals after Explosive Shock," Transactions of the Metallurgical Society of AIME, Oct., 1958, pp. 274-289
3. C. S. Smith and C. M. Fowler, "Further Metallographic Studies of Metals after Explosive Shock," Response of Metals to High Velocity Deformation, Interscience Publishers, New York, 1961, p. 309
4. J. M. Walsh, M. H. Rice, R. G. McQueen, and F. L. Yarger, "Shock Wave Compression of 27 Metals, Equations of State for Metals," Physical Review, 1957, vol. 108, p. 203
5. W. E. Drummond, "Multiple Shock Production," Journal of Applied Physics, 1957, vol. 28. pp. 998-1001
6. J. Taylor, Detonation in Condensed Explosives, Oxford University Press, London, 1952, p. 82
7. W. E. Deal, "Measurement of the Reflected Shock Hugoniot and Isentrope for Explosion Reaction Products," Physics of Fluids, vol. I, 1958, p. 524
8. R. W. Tomlinson, "Properties of Explosives of Military Interest," 1st. Revision by O. E. Sheffield, Picatinny Arsenal Report No. 1740, April, 1958
9. O. E. Sheffield, "Properties of Explosives of Military Interest, Supplement I," Picatinny Arsenal Report No. 1740, August, 1958
10. S. Katz, D. G. Doran, and D. R. Curran, "Hugoniot Equation of State of Aluminum and Steel from Oblique Shock Measurement," Journal of Applied Physics, 1959, vol. 30, p. 573
11. J. O. Erkman, "Explosively Induced Nonuniform Oblique Shocks," Technical Report No. 17, Contract No. DA-04-200-509-ORD-294, Stanford Research Institute, June 3, 1958, pp. 13, 16

12. J. O. Erkman, "Decay of Explosively-Induced Shock Waves in Solids and Spallings of Aluminum," Third Symposium on Detonation, Princeton University, September 26-28, 1960, p. 265
13. G. E. Duvall, "Some Properties and Applications of Shock Waves," Poulter Laboratories Technical Report 006-60, Stanford Research Institute, October 17, 1960, p. 16

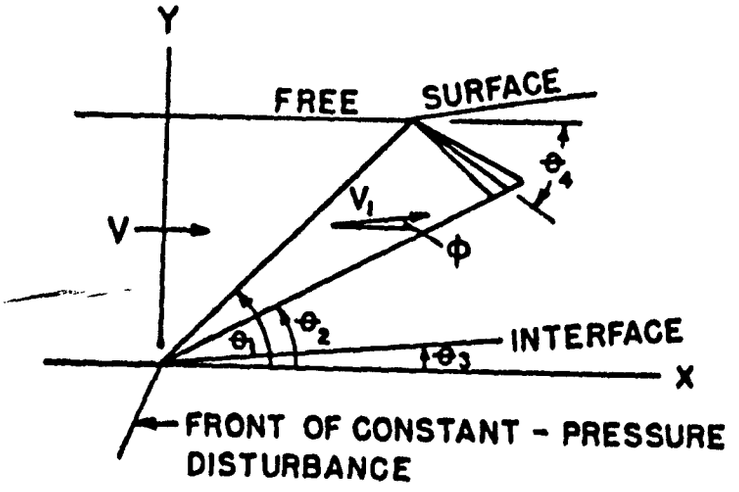

FIG. 1 OBLIQUE LOADING OF IRON PLATE

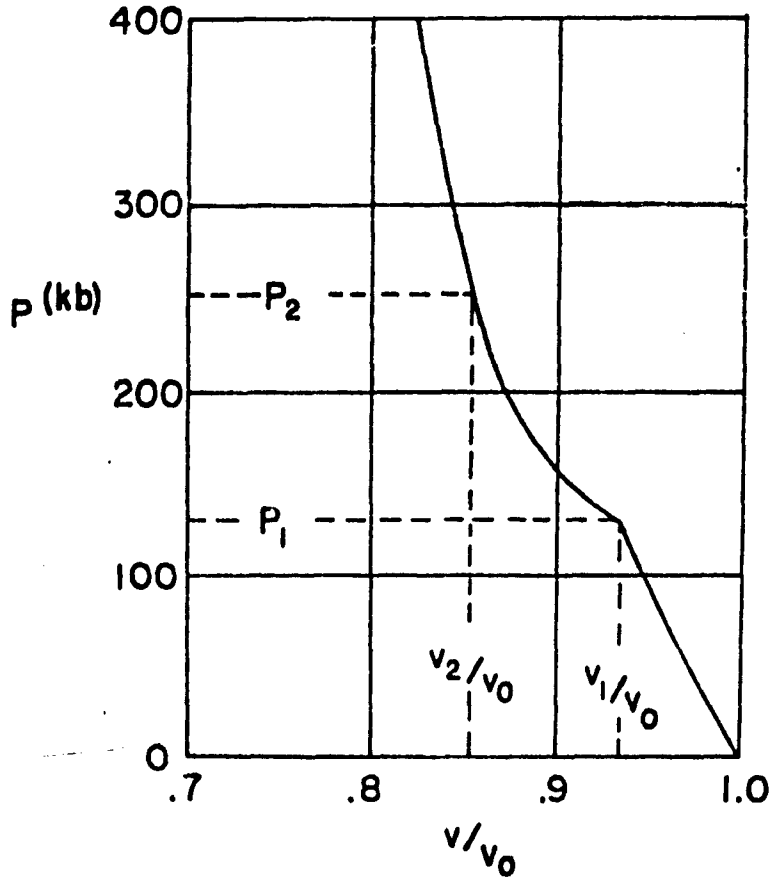

FIG. 2 HUGONIOT FUNCTION FOR IRON
(REFERENCE 4)

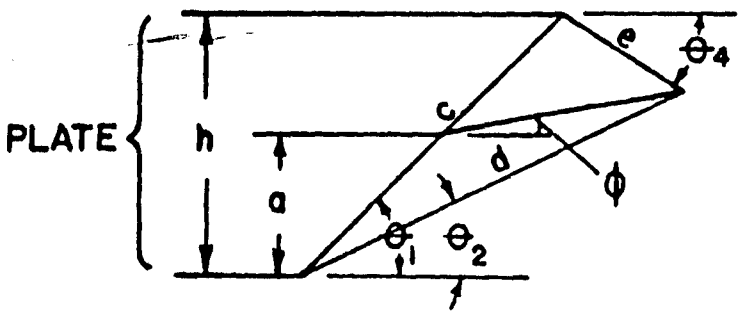

FIG. 3 . GEOMETRY OF INTERACTION ZONE FORMATION

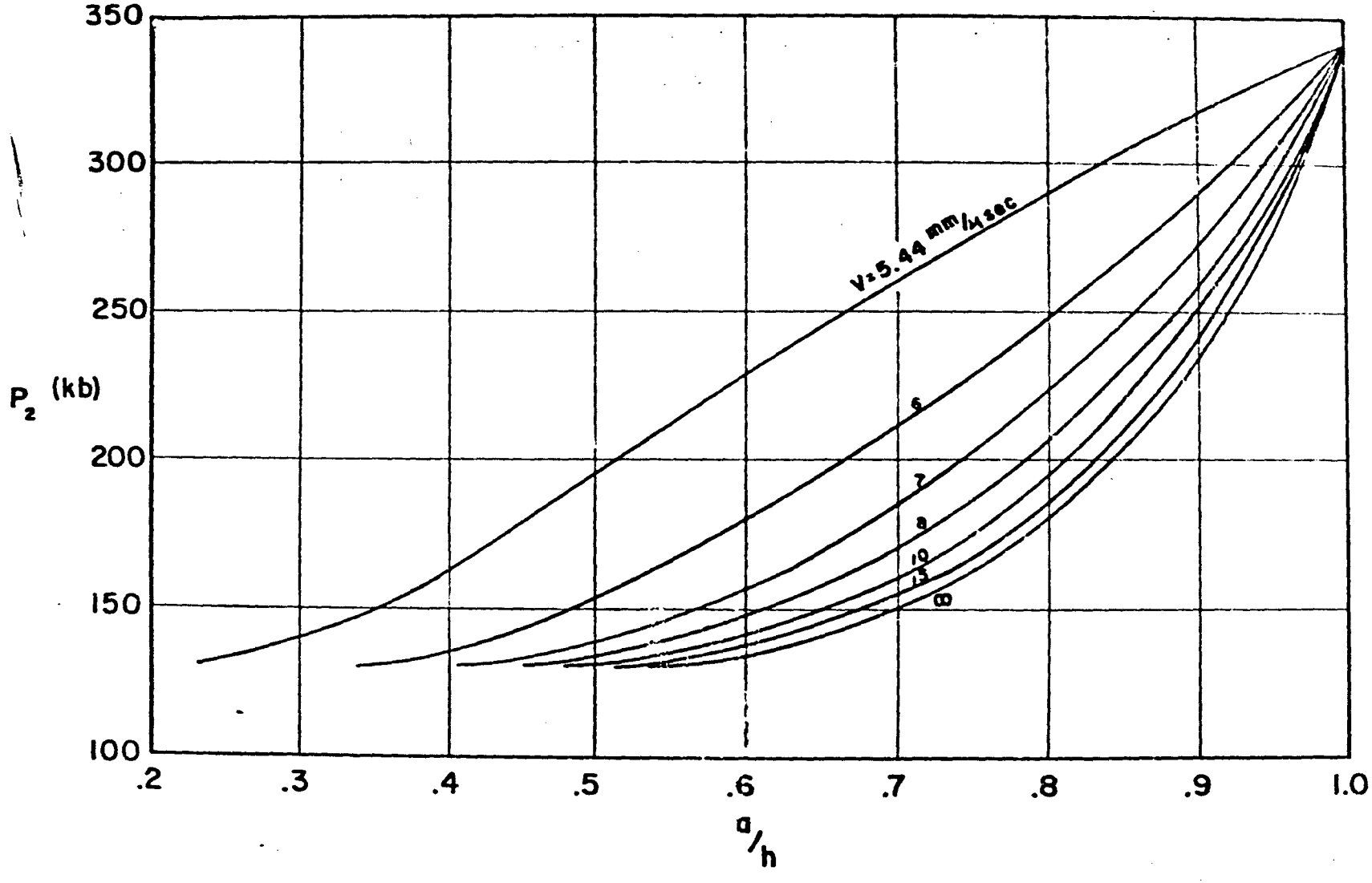

FIG. 4 INDUCED PRESSURE AS FUNCTION OF a/h AND V

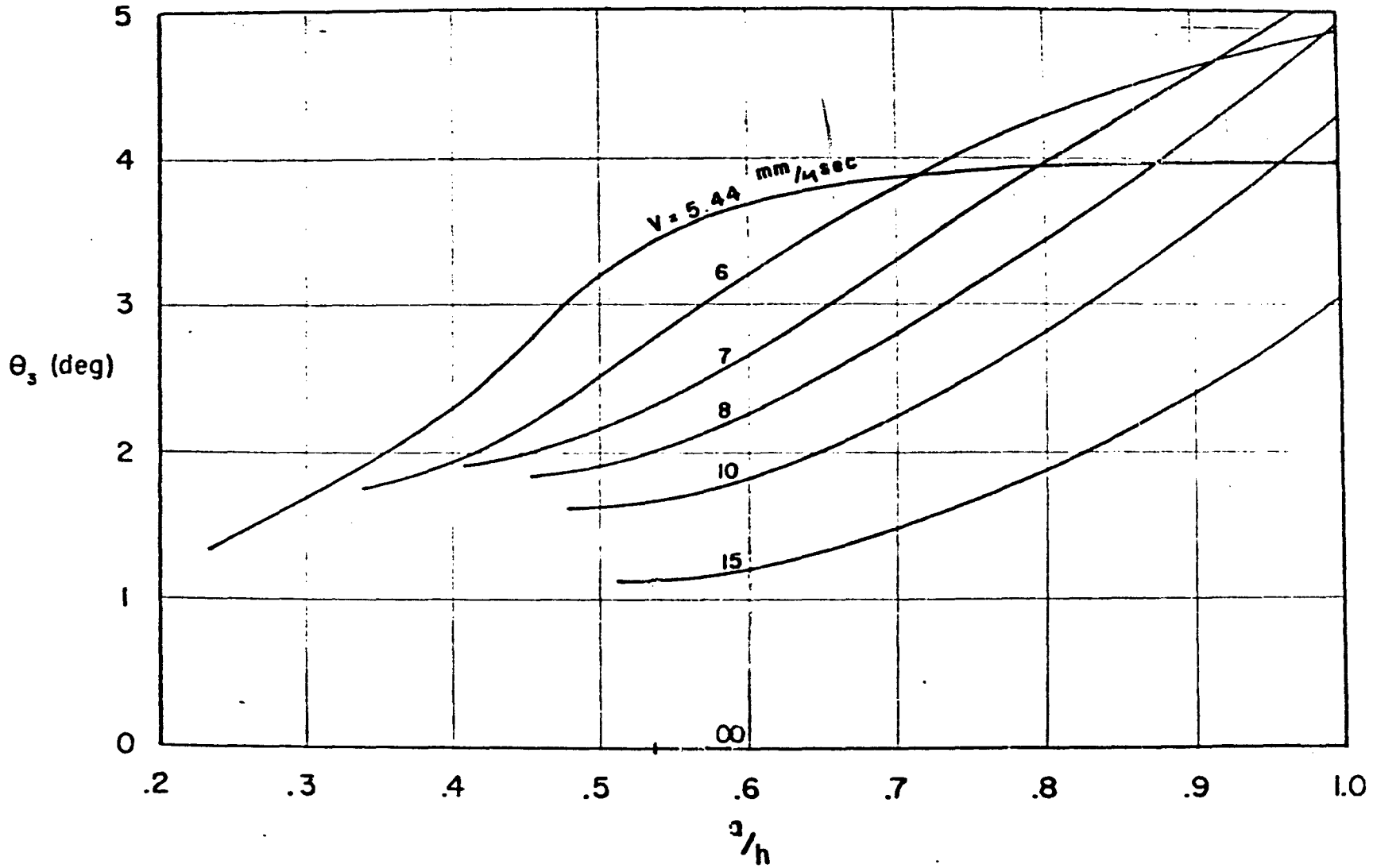

FIG. 5 INTERFACE ROTATION AS FUNCTION OF a/h AND V

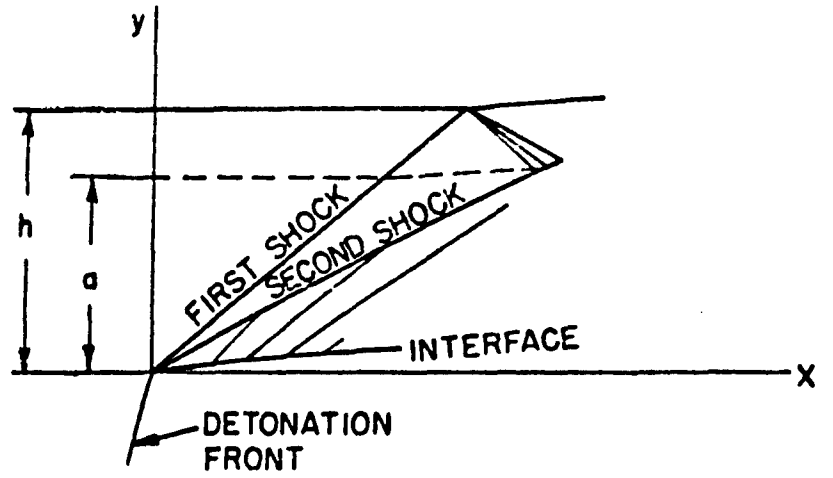

CASE 1

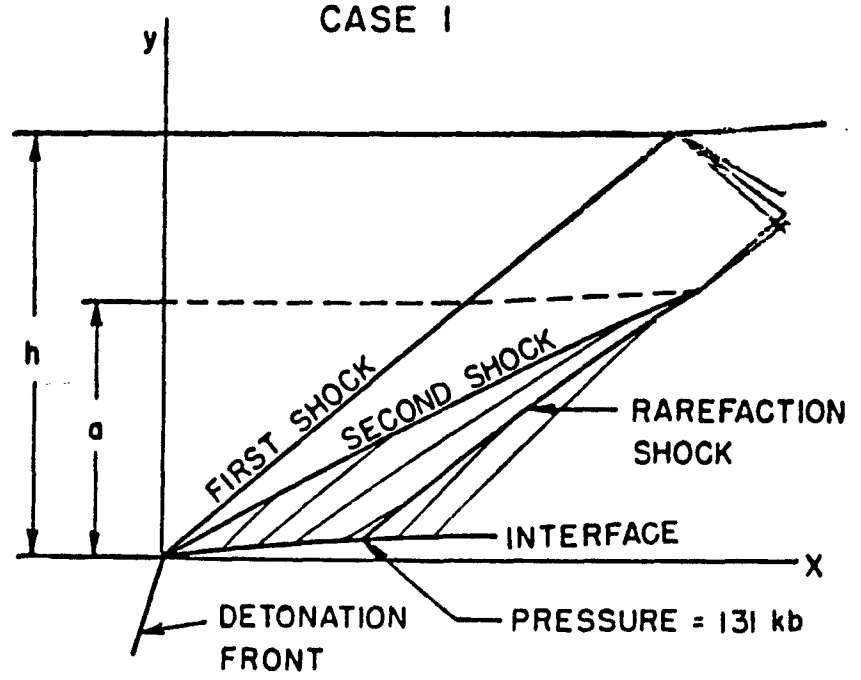

CASE 2

FIG. 6 WAVE PATTERNS INDUCED BY OBLIQUE DETONATION

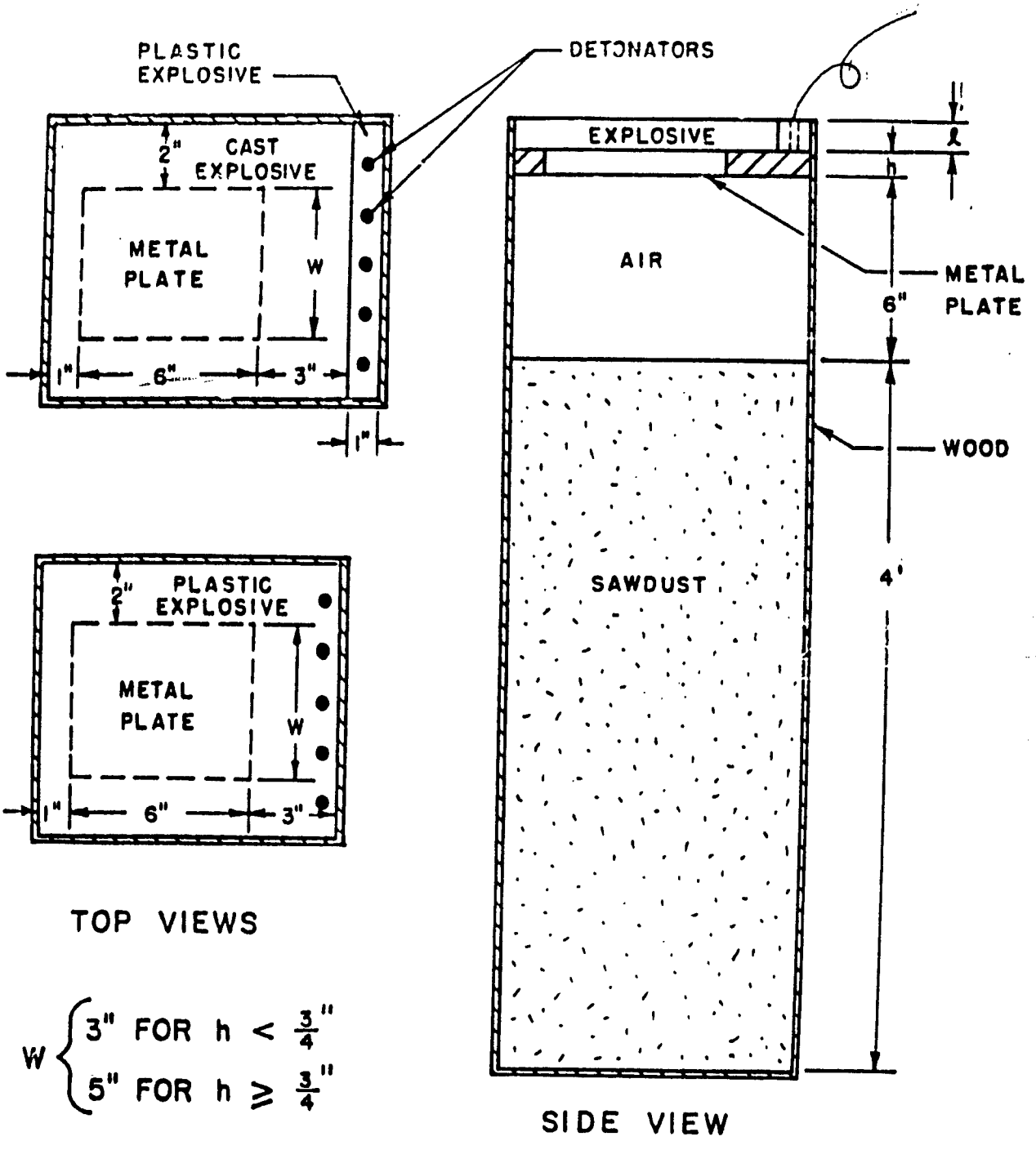

FIG. 7 ARRANGEMENTS FOR OBLIQUE LOADING WITH PLASTIC AND CAST EXPLOSIVES

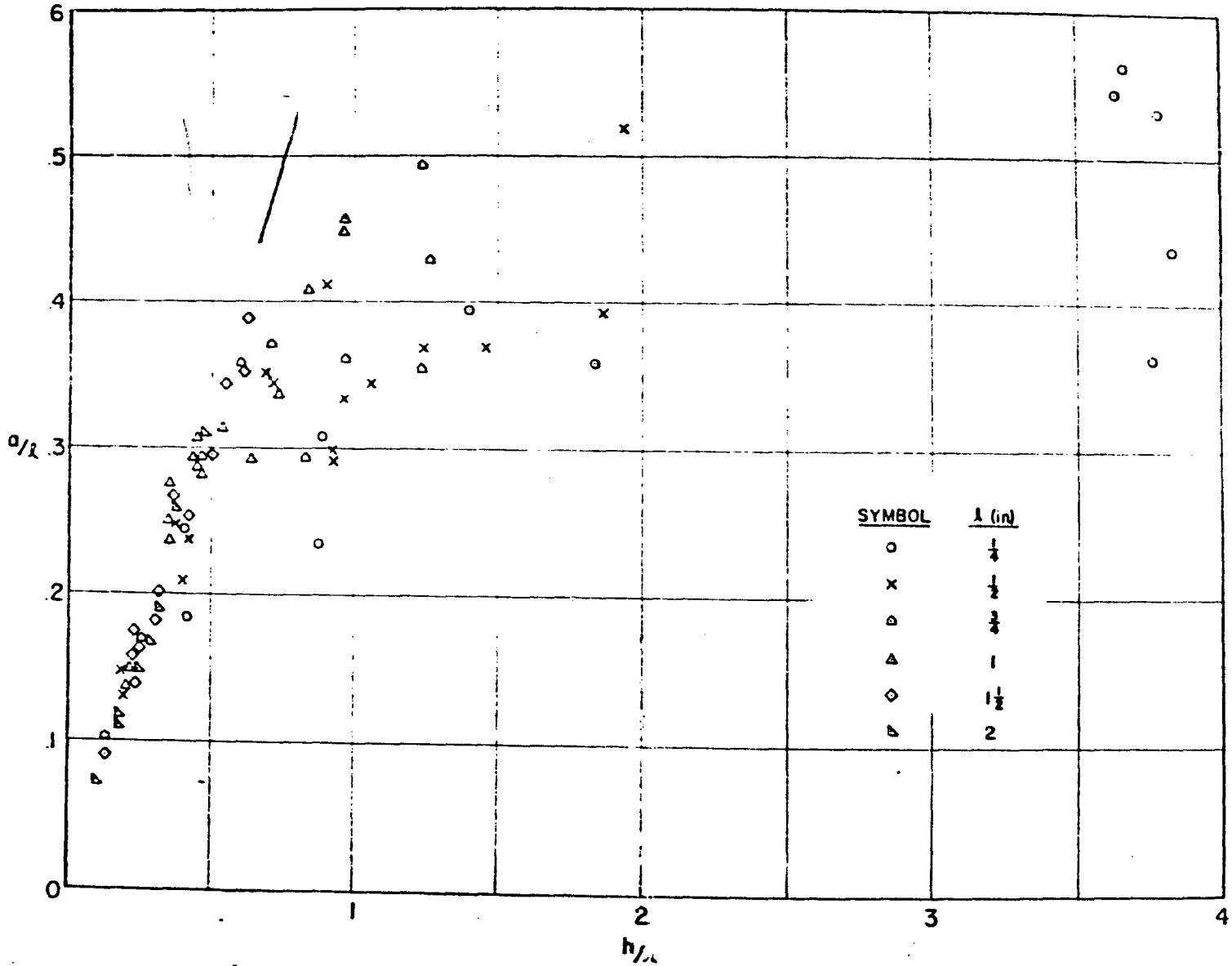

FIG. 8 HARDENED ZONE THICKNESS FOR COMPOSITION C-3

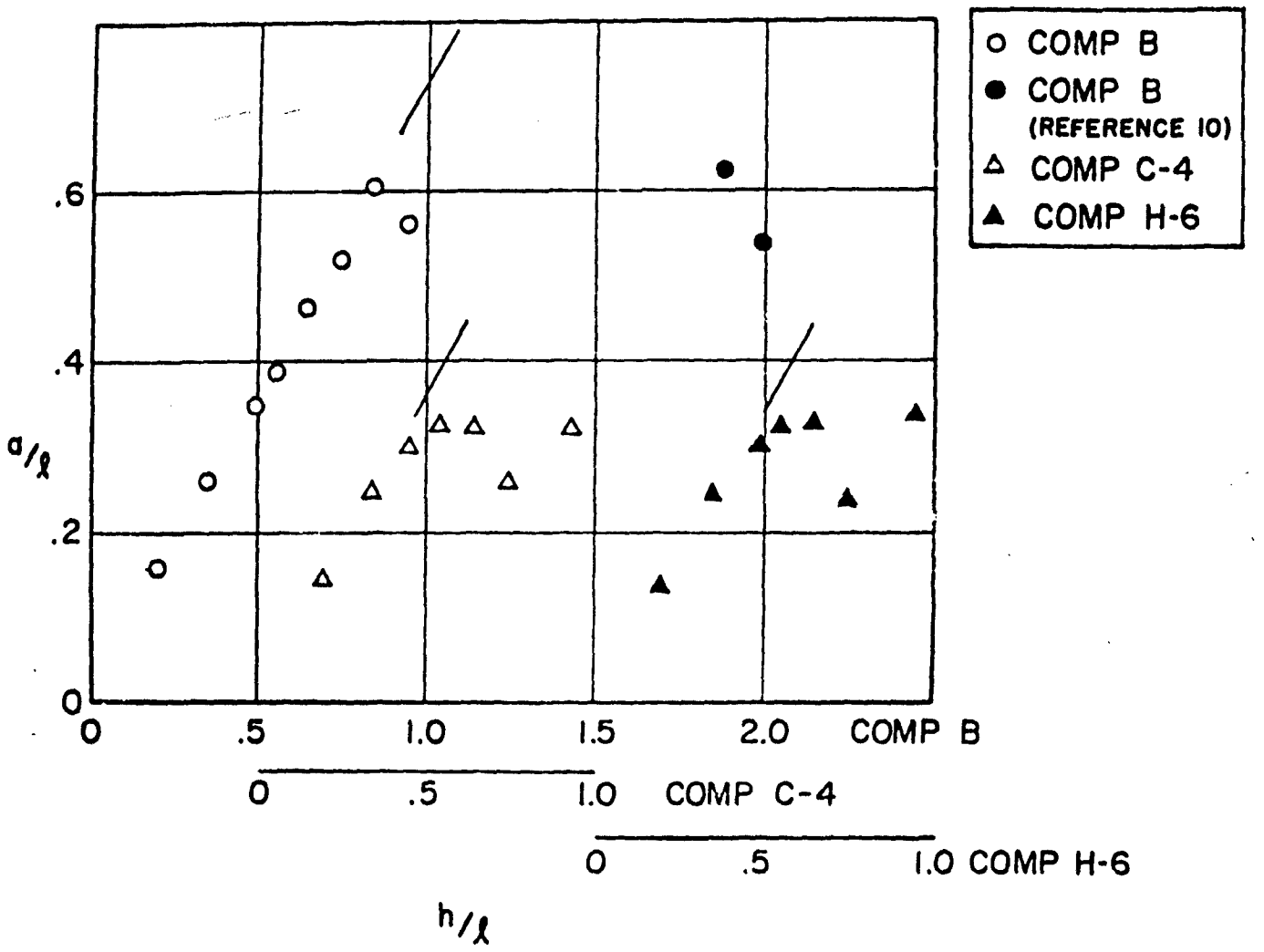

FIG. 9 HARDENED ZONE THICKNESS FOR THREE EXPLOSIVES

APPENDIX A

TABULATION OF EXPERIMENTAL DATA

All dimensions are in inches. Asterisks denote plates of Armco iron. The remainder of the plates are steel with carbon content between .15% and .28%.

1. Composition C-3 Explosive

Explosive Thickness	Original Plate Thickness	Final Plate Thickness	Measured Hardened Zone	Corrected Hardened Zone
.244	.100*	.097	.058	.060
.239	.099	.101	.145	.044
.242	.216	.216	.074	.074
.245	.218	.220	.058	.057
.250	.351*	.342	.096	.098
.250	.462	.459	.089	.090
.256	.939	.936	.144	.144
.257	.936	.935	.140	.140
.250	.957	.958	.109	.109
.253	.956	.941	.090	.091
.250	.948	.924	.130	.133
.502	.098*	.081	.062	.075
.502	.099	.099	.066	.066
.499	.200*	.200	.104	.104
.512	.215	.214	.121	.121
.500	.199	.195	.121	.124
.499	.350*	.348	.171	.172
.510	.355	.352	.177	.178
.501	.464*	.463	.148	.148
.508	.462*	.440	.198	.208
.407	.458	.453	.143	.145
.498	.486	.489	.167	.166
.518	.552	.551	.178	.178
.521	.650	.644	.189	.191
.522	.751	.710	.181	.192
.499	.936	.936	.196	.196
.492	.956	.899	.239	.254
.760	.099	.100	.080	.079
.741	.197	.210	.134	.126
.758	.351*	.334	.205	.216
.754	.356	.350	.216	.220
.740	.456	.441	.255	.264
.770	.552	.536	.278	.286
.772	.648	.643	.224	.225

TABULATION OF EXPERIMENTAL DATA (Continued)

1. Composition C-3 Explosive (Continued)

Explosive Thickness	Original Plate Thickness	Final Plate Thickness	Measured Hardened Zone	Corrected Hardened Zone
.772	.752	.746	.276	.278
.738	.939	.738	.314	.314
.766	.956	.941	.373	.378
.766	.956	.917	.261	.271
.981	.198*	.183	.123	.133
1.010	.197	.191	.145	.150
.988	.350*	.334	.234	.245
.991	.356	.351	.268	.272
1.003	.352	.339	.227	.236
1.013	.470*	.452	.276	.287
.997	.456	.435	.291	.305
1.040	.458*	.440	.294	.306
1.009	.648	.633	.288	.295
.972	.936	.890	.415	.436
.985	.956	.908	.427	.449
1.019	.851	.859	.420	.416
1.018	.749	.738	.339	.344
1.010	.552	.529	.304	.317
1.497	.198	.197	.134	.135
1.505	.350*	.335	.199	.208
1.504	.356	.327	.225	.245
1.486	.354	.327	.235	.254
1.487	.351	.326	.223	.239
1.496	.458	.418	.248	.271
1.504	.486	.465	.290	.303
1.509	.552	.500	.364	.401
1.522	.648	.601	.359	.387
1.502	.749	.720	.422	.438
1.516	.847	.820	.506	.521
1.501	.936	.906	.512	.528
1.500	.956	.931	.567	.582
2.008	.199	.186	.140	.150
2.006	.350*	.325	.209	.225
2.011	.351	.317	.212	.235
2.013	.486	.435	.267	.298

TABULATION OF EXPERIMENTAL DATA (Continued)

1. Composition C-3 Explosive (Continued)

Explosive Thickness	Original Plate Thickness	Final Plate Thickness	Measured Hardened Zone	Corrected Hardened Zone
2.016	.552	.485	.295	.337
2.008	.650	.584	.343	.382
2.006	.752	.699	.482	.520
2.052	.956	.894	.593	.634

2. Composition C-4 Explosive

.997	.198	.193	.145	.149
1.009	.356	.342	.239	.248
.993	.456*	.437	.288	.300
1.007	.552	.534	.318	.329
1.011	.649	.630	.316	.325
1.008	.750	.747	.260	.261
.998	.936	.934	.320	.321

3. Composition B Explosive

1.022	.199	.197	.161	.163
1.022	.353	.347	.276	.280
1.022	.486	.467	.331	.345
1.024	.650	.634	.454	.468
1.022	.749	.738	.514	.522
1.021	.957	.925	.547	.566
1.022	.552	.531	.382	.391
1.023	.849	.836	.604	.613

4. Composition H-6 Explosive

1.035	.199	.178	.121	.135
1.015	.351	.340	.237	.245
1.020	.486	.442	.301	.331
1.037	.648	.622	.332	.346
1.015	.747	.734	.231	.235
1.020	.956	.901	.324	.344
1.035	.552	.552	.320	.320

APPENDIX B

DISTRIBUTION

Bureau of Naval Weapons

DLI-31	4
R-12	1
RMMO	1
RMMO-5	1
RMMO-52	1
RMMO-512	1
RUME-32	1
RUME-323	1

Commander
Armed Forces Technical Information Agency
Arlington Hall Station
Arlington 12, Virginia
Attn: TIPDR — 10

Commander, Operation Test and Evaluation Force
U. S. Atlantic Fleet, U. S. Naval Base
Norfolk 11, Virginia — 1

Office of Technical Services
Department of Commerce
Washington 25, D. C. — 1

Commander
Naval Ordnance Laboratory
Corona, California
Attn: Technical Library — 1

Commander
Naval Ordnance Test Station
Pasadena Annex
Pasadena, California
Attn: Library — 1

Commander
Naval Ordnance Test Station
China Lake, California
Attn: Mr. John Pearson — 1
Attn: Technical Library Branch — 1

Commander
Naval Ordnance Laboratory
White Oak, Silver Spring, Maryland
Attn: Library — 2
Attn: ED Division — 1

DISTRIBUTION (Continued)

Commander
U. S. Naval Nuclear Ordnance Evaluation Unit
Kirtland Air Force Base
Albuquerque, New Mexico
Attn: Mr. E. B. Massengill — 1

Director
Naval Research Laboratory
Anacostia 20, D. C. — 1

Officer-In-Charge
Naval Weapons Station
Yorktown, Virginia — 1

Commanding Officer
Office of Ordnance Research
Box CM
Duke Station
Durham, North Carolina — 1

Commanding Officer
Picatiny Arsenal
Dover, New Jersey
Attn: Library — 1

Commanding General
Aberdeen Proving Ground
Aberdeen, Maryland
Attn: Library — 1
Attn: Technical Information Section
Development and Proof Services — 2

Los Alamos Scientific Laboratory
Los Alamos, New Mexico
Attn: Dr. C. M. Fowler — 1
Attn: Dr. J. M. Walsh — 1
Attn: Dr. W. E. Deal — 1
Attn: Library — 1

Battelle Memorial Institute
Defense Metals Information Center
Columbus 1, Ohio — 2

DISTRIBUTION (Continued)

The Institute for the Study of Rate Processes
University of Utah
Salt Lake City, Utah
Attn: Explosives Research Group 1

Stanford Research Institute
Poulter Laboratories
Menlo Park, California
Attn: Dr. G. E. Duvall 1
Attn: Dr. J. O. Erkman 1
Attn: Dr. S. Katz 1
Attn: Library 1

Institute for the Study of Metals
The University of Chicago
5640 Ellis Avenue
Chicago 37, Illinois
Attn: Dr. C. S. Smith 1

Applied Physics Laboratory
Johns Hopkins University
Silver Spring, Maryland 2

Director
Franklin Institute
20th Street and Benjamin Franklin Parkway
Philadelphia 3, Pennsylvania 1

British Joint Services Mission
The BNS/MOSS Scientific and Technical Information Section
P. O. Box 680, Benjamin Franklin Station
Washington, D. C.
Attn: Technical Information Officer
Via: BUWEPS (DSC) 4

Defense Research Member
Canadian Joint Staff (W)
2450 Massachusetts Avenue, N. W.
Washington 8, D. C.
Attn: Dr. H. P. Tardiff, CARDE, Quebec (1)
Via: BUWEPS (DSC) 4

DISTRIBUTION (Continued)

Sandia Corporation
Sandia Base
Albuquerque, New Mexico
Attn: Dr. F. W. Neilson 1

General Electric Company
Syracuse, New York
Attn: Dr. F. A. Lucy 1

Sandia Corporation
Livermore, California
Attn: Technical Library 1

Colorado School of Mines
Golden, Colorado
Attn: Dr. John S. Rinehart 1

E. I. duPont de Nemours and Company, Inc.
Wilmington, Delaware
Attn: Dr. G. E. Dieter 1
Attn: Dr. G. R. Cowan 1
Attn: Dr. A. H. Holtzman 1

Local:

D	1
T	1
TX	4
TD	1
TDMM-3	1
TDMM-4	1
TR	1
TRE-1	1
TRE-2	3
ACL	5
File	1

Naval Weapons Lab. (NWL Report No. 1786)
EXPLOSIVE-INDUCED PRESSURES IN IRON, by William G. Soper and Lester A. Potteiger. 22 Nov 1961. 14 p., 9 figs., 3 tables.
UNCLASSIFIED

A metallographic technique is discussed for determining the level of pressure to which iron plates have been subjected by explosive loading. The interaction of the shock and rarefaction waves within the plate is analyzed to arrive at formulas from which the intensity of pressure can be determined when the velocity of the detonation front is known. This technique is employed to determine the pressure induced in iron by oblique detonation of four common explosives, Compositions B, C-3, C-4, and H-6.

1. Iron - Shock resistance
2. Explosive loading
I. Soper, W. G.
II. Potteiger, L. A.
III. Title
IV. NAVWEPS 7669

Task: R01101001

UNCLASSIFIED

Naval Weapons Lab. (NWL Report No. 1786)
EXPLOSIVE-INDUCED PRESSURES IN IRON, by William G. Soper and Lester A. Potteiger. 22 Nov 1961. 14 p., 9 figs., 3 tables.
UNCLASSIFIED

A metallographic technique is discussed for determining the level of pressure to which iron plates have been subjected by explosive loading. The interaction of the shock and rarefaction waves within the plate is analyzed to arrive at formulas from which the intensity of pressure can be determined when the velocity of the detonation front is known. This technique is employed to determine the pressure induced in iron by oblique detonation of four common explosives, Compositions B, C-3, C-4, and H-6.

1. Iron - Shock resista
2. Explosive loading
I. Soper, W. G.
II. Potteiger, L. A.
III. Title
IV. NAVWEPS 7669

Task: R01101001

UNCLASSIFIED

Naval Weapons Lab. (NWL Report No. 1786)
EXPLOSIVE-INDUCED PRESSURES IN IRON, by William G. Soper and Lester A. Potteiger. 22 Nov 1961. 14 p., 9 figs., 3 tables.
UNCLASSIFIED

A metallographic technique is discussed for determining the level of pressure to which iron plates have been subjected by explosive loading. The interaction of the shock and rarefaction waves within the plate is analyzed to arrive at formulas from which the intensity of pressure can be determined when the velocity of the detonation front is known. This technique is employed to determine the pressure induced in iron by oblique detonation of four common explosives, Compositions B, C-3, C-4, and H-6.

1. Iron - Shock resistance
2. Explosive loading
I. Soper, W. G.
II. Potteiger, L. A.
III. Title
IV. NAVWEPS 7669

Task: R01101001

UNCLASSIFIED

Naval Weapons Lab. (NWL Report No. 1786)
EXPLOSIVE-INDUCED PRESSURES IN IRON, by William G. Soper and Lester A. Potteiger. 22 Nov 1961. 14 p., 9 figs., 3 tables.
UNCLASSIFIED

A metallographic technique is discussed for determining the level of pressure to which iron plates have been subjected by explosive loading. The interaction of the shock and rarefaction waves within the plate is analyzed to arrive at formulas from which the intensity of pressure can be determined when the velocity of the detonation front is known. This technique is employed to determine the pressure induced in iron by oblique detonation of four common explosives, Compositions B, C-3, C-4, and H-6.

1. Iron - Shock resista
2. Explosive loading
I. Soper, W. G.
II. Potteiger, L. A.
III. Title
IV. NAVWEPS 7669

Task: R01101001

UNCLASSIFIED